Study on the Geotechnical Properties Changes of Loess after Seismic Landslides: A Case Study of the Subao Loess Landslide in Ningxia, China

Da Peng *, Jingshan Bo , Chaoyu Chang , Xiaobo Li , Yushi Duan , Wenhao Qi

Posted Date: 7 September 2023

doi: 10.20944/preprints202309.0502.v1

Keywords: Undisturbed loess; Landslide deposit; Grain size distribution,; Consolidation; Dynamic Shear Modulus

Article

Study on the Geotechnical Properties Changes of Loess after Seismic Landslides—A Case Study of the Subao Loess Landslide in Ningxia, China

Da Peng [1,*], Jingshan Bo [1,2,3], Chaoyu Chang [2,3], Xiaobo Li [1], Yushi Duan [1,2,3] and Wenhao Qi [1]

[1] Key Laboratory of Earthquake Engineering and Engineering Vibration, Institute of Engineering Mechanics, China Earthquake Administration, Harbin 150080, China;
[2] Hebei Key Laboratory of Earthquake Disaster Prevention and Risk Assessment, Sanhe 065201, China;
[3] Institute of Disaster Prevention, Institute of Geological Engineering, Sanhe 065201, China

Abstract: This study aims to explore the differences between loess and landslide deposits, focusing on aspects such as particle distribution, consolidation characteristics, and dynamic shear modulus. Through a series of experiments, the research reveals the similarities and differences between these two entities, yielding several key findings. Firstly, the process of landsliding disrupts the original structure of the loess, resulting in a reduction in porosity and a densification of the soil. This alteration in structural properties leads to significant disparities in physical attributes between landslide deposits and undisturbed loess. Additionally, the movement and sorting of particles during landslides cause variations in particle size distribution across different sections of the landslide deposits. Secondly, the landslide process not only alters the soil's structure but also changes the particle sizes within the loess. Particle wear and sieving result in the transformation of larger particles into smaller ones, leading to a more uniform particle size distribution. This shift in structure and particle size directly impacts the consolidation characteristics of landslide deposits, resulting in a substantial reduction in compression coefficient. Despite undergoing consolidation for decades, the middle and lower sections of landslide deposits still exhibit under-consolidation. Although the differences in the maximum dynamic shear modulus between loess and landslide deposits at varying depths are relatively minor, differences in porosity and consolidation characteristics lead to faster decay rates of the dynamic shear modulus for the latter. The study also highlights a reduction in the water sensitivity of the maximum dynamic shear modulus within landslide deposits. Based on experimental results, a predictive model is proposed, utilizing A and m values to estimate the maximum dynamic shear modulus of both loess and landslide deposits. In conclusion, this research uncovers the impact of landslide processes on the structure and properties of loess, providing insightful understanding into the disparities between these two entities.

Keywords: undisturbed loess; landslide deposit; grain size distribution; consolidation; dynamic shear modulus

1. Introduction

The Loess Plateau in China is located in the middle and upper reaches of the Yellow River. It stretches from the Riyue Mountain, Helan Mountain, and Wusha-oling in the west to the Taihang Mountain Range in the east. It is bordered by the Great Wall to the north and reaches the Qinling Mountains to the south [1]. Due to tectonic movement and soil erosion, the Loess Plateau features a landscape of undu-lating hills and crisscrossing gullies. In history, the Loess Plateau has experienced 7 earthquakes with a magnitude of 7.5 or above (including magnitude 7.5) and 20 earthquakes with magnitudes between 7 and 7.5, resulting in over 1.4 million casual-ties. It is noteworthy that these strong earthquakes have triggered numerous loess earthquake landslides with diverse forms and widespread distribution. The casualties caused by loess earthquake landslides account for 1/3 to 2/3 of the total number of casualties [2]. On December 16, 1920, a M 8.5 earthquake occurred in the Ningxia Haiyuan, China, which induced more than 7000 landslides [3]. About 100,000 people were killed by those landslides [4], and the area >200 km^2 was covered by sliding zone and depositions

[5,6]. The typically earthquake-induced loess landslides are large-scale, long run-out, low angle sloping source (<20°) and flat depositions [7–9].

As a typically homogeneous, non-stratified and highly porous silty soil, loess, especially Q_3 loess, may produce liquefaction, seismic subsidence, fragmentation with strong seismic motion [10–13]. Thus, many potential mechanisms of earthquake-induced loess landslides have been proposed. Some researchers indicated that loess disintegrates into dry loess flow under strong ground motion, and rapidly travel with high pore air pressure [14,15]. Wang and Zhang [15] reported that the void ratio of deposition soil is 1.2~1.3 times of that of undisturbed loess of sliding source. Another view is seismic subsidence. Microscopically, the particles at the connection point of the dry loess microstructure will shift under the vibration, leading to microscopic damage, which may spread along the sliding surface and lead to overall deformation and damage; Macroscopically, Slopes build of such dry loss tend to collapse and seismic [16]. Zhang and Wang [8] indicated that the void ratio is an important index to evaluate this change. The common view is that loess liquefaction occurred in those landslides [17–20]. Some experimental cases showed that when the saturation of loess is high, the loess has obvious liquefaction potential [21–23]. Tests and field investigations have shown that the physical and mechanical properties of soil change greatly with landslide process [24,25]. The changes in the physical and mechanical properties of landslide source and slide deposits indicate the mechanism of landslide and landslide runout process [26,27].

During landslide field investigation of the 1920 Haiyuan *M*8.5 earthquake, we found that there were a large number of loess sheets, loess gravel, and discontinuous surface structures such as fracture surfaces, shear surfaces and directional arrangement in the landslide deposits. These phenomena show that pressure and slip process in landslide runout. In order to explore the changes of physical, mechanical and dynamic properties of loess during earthquake landslide movement, so as to understand the formation mechanism and movement process of loess co-seismic landslide. In this study, A typical loess earthquake landslide, Subao landslide, was selected as the example to analyze the changes of landslide source with slide deposit. Drillings and well explorations were used to get profile of landslide source and deposit and take undisturbed soil sample from landslide source and deposit. A series of tests were conducted to present the basic physical properties, compressibility coefficient, dynamic shear modulus at different depths. Thereby, This holds great significance for a thorough understanding of the physical property changes in loess during the process of landslide movement.

2. Test materials and methods

2.1. Study site

Subao landslide is located approximately 25 km southwest of Xiji city, Ningxia Hui Autonomous Region, China. The shortest distance from the study site to the seismogenic fault Haiyuan fault zone is about 62 km, which is in level IX area of 1920 Haiyuan earthquake [7]. An overview of the study site as shown in Figure 1(a). The boundary between landslide accumulation mass and landslide is clear. The deposit is flat with a gradient of 2°. The middle and upper part of the deposit is farmland with slight disturbance, and the lower part is village, with serious disturbance. The front part of the deposit moved along the muddy river to both sides, and formed Subao dammed Lake with the sliding mass of the Hongtuchuan landslide on the opposite side. Figure 1(b) present the topography of the landslide area. The landslide has a maximum width of about 360 m and a length of 1320 m. The thicknesses of deposit were inferred to be approximately 20~45m in different area, and average deposit thickness is 30 m. Respectively, the total volume of Subao landslide is about 1.2×10^7 m^3. The main scrap the landslide is high and steep, with a height of 80m and gradient of 50°. We found mudstone exposed under the main scrap. Our observations suggest that the movement type of the landslide is translational sliding based on Varnes' classification system [14] and the type is loess-bedrock Interface slide based on Li' classification system [28].

Preprints (www.preprints.org) | NOT PEER-REVIEWED | Posted: 7 September 2023 doi:10.20944/preprints202309.0502.v1

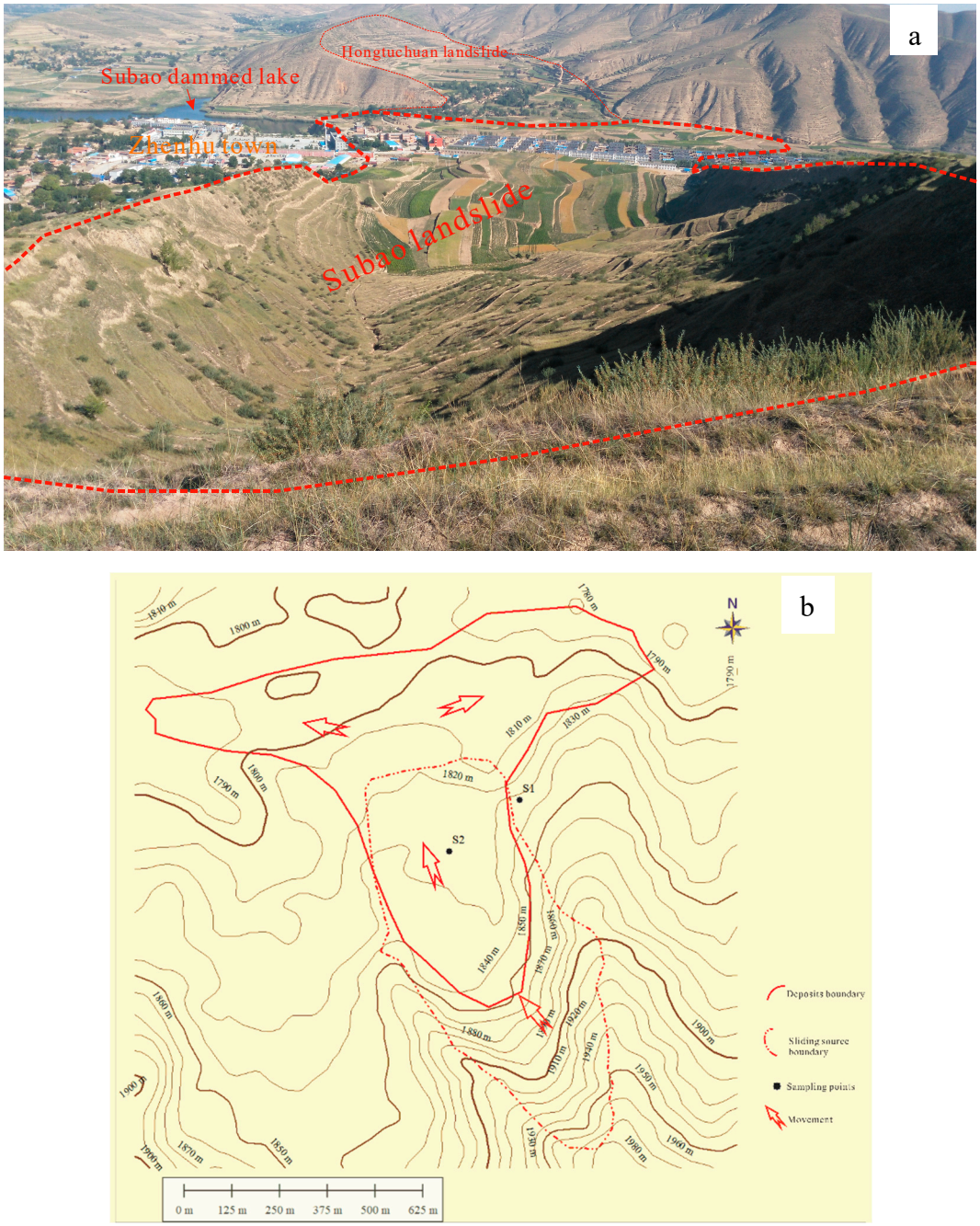

Figure 1. (a)The Subao loess landslide. (b) Engineering geological map of Subao landslide.

2.2. Sample preparation and experimental equipment

Loess is a kind of soil which is sensitive to pressure, water and vibration, and is easily disturbed. In order to make loess undisturbed as much as possible, we excavated two exploratory wells on the left side of the sliding source. The location of the exploratory well is shown in Figure 2, with a diameter of 0.8m. Then, large pieces of loess samples are cut from side of well and brought to the ground to be cut. A cylindrical soil block with dimensions of 160mm×300mm was cut carefully along vertical direction from large pieces using the method of manual trimming. The gap between the sample and the cylinder container be filled with the loose soil left after cutting. Immediately, containers containing loess samples were sealed to prevent water loss. In order to prevent vibration interference during transportation, sponge be used between cylinder containers.

Preprints (www.preprints.org) | NOT PEER-REVIEWED | Posted: 7 September 2023 doi:10.20944/preprints202309.0502.v1

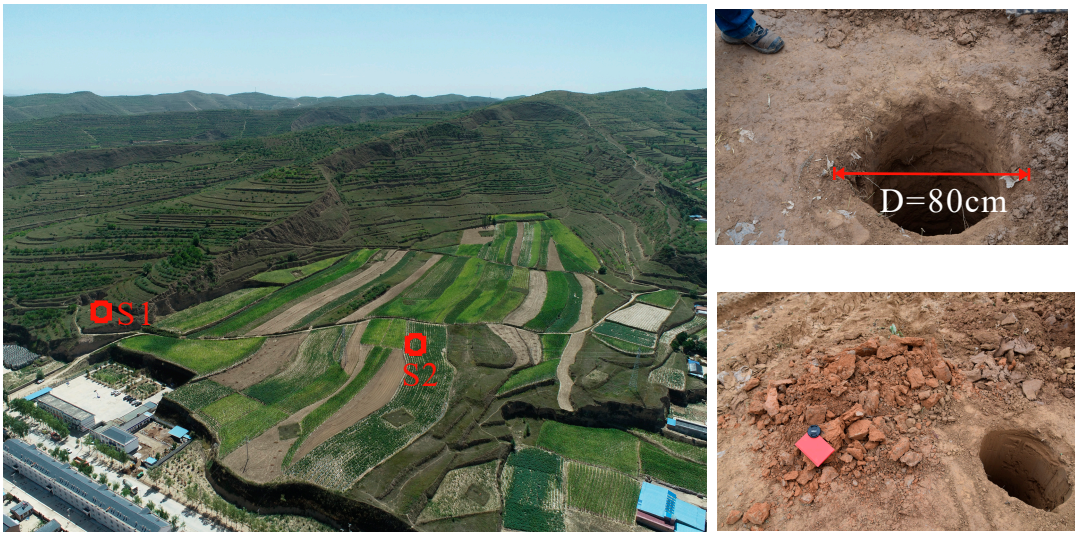

Figure 2. Sampling locations of undisturbed loess (S1) and landslide deposit soil samples (S2).

The soil profiles of landslide source and deposition are shown in Figure 3 with the corresponding sample points and shear wave velocity (Vs). The top elevation of S1 is 1871m with 34m of soil. Apart from a thickness of 1.6m top cultivated soil layer, a thickness of uniform loess is about 32m, which is commonly designated as Q_3 loess (Malan loess) based on formation age and physical properties. The lower part is mudstone, which is Low permeability and high strength. Stable groundwater level is 30m below the ground. We sampled at the depth of 4m, 6m, 10m, 16m, 20m, 24m, 30m respectively, and the number is S04, S06, S10, S16, S20, S24, S30. The upper part of the S2 is cultivated soil with a thickness of 1.8m, and the lower part is loess-like soil with a thickness of 35m. Similarly, stable groundwater level is 30m below the ground. The depth of 2m, 4m, 7m, 10m, 13m,18m, 20m, 24m, 30m soils were sampled respectively, and the number is D02, D04, D07, D10, D13, D18, D20, D24, D30. In addition, shear wave velocity tests of two pit were conducted by signal hole method. The results as shown in Figure 3 present the shear wave velocity increases rapidly from ground to depth of 7m and oscillation increases slowly below depth of 7m in S1. The average shear wave velocity in the upper 30 m (V_S30) is 306m/s. And, the shear wave velocity increases from ground to depth of 14m and oscillation increases slowly below depth of 14m in S12. The average shear wave velocity in the upper 30 m (V_S30) is 288m/s.

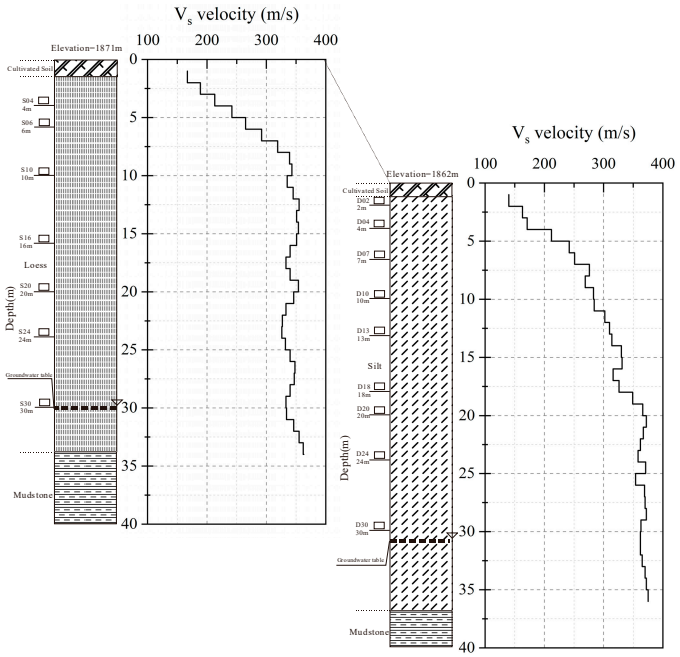

Preprints (www.preprints.org) | NOT PEER-REVIEWED | Posted: 7 September 2023 doi:10.20944/preprints202309.0502.v1

Figure 3. soil profile of sampling site (Vs values are measured through down-hole tests).

In this study, a series of laboratory tests were conducted. Table 1 shows the summary of laboratory tests and standards for soil properties. Due to the unique macro pore and sub stable microstructure of loess, the disturbance may have a serious impact on the mechanical properties of soil mass. Therefore, the sample preparation should be conducted carefully in strict accordance with the established sample preparation standards to ensure that high-quality loess samples are obtained. The resonant column test adopts the GDS-RCA resonant column test system [29], the test sample specifications are 50 mm in diameter and 100 mm in height.

Table 1. The summary of laboratory tests and standards for soil properties.

Index properties	Standard	Parameters determined	Samples
Density, dry density	ASTM D7263	γ, γ_d	all
Initial void ratio		e	all
Specific gravity	ASTM D854	G_s	all
Grain size	ASTM D422, D1140	D_{60}, D_{50}, D_{30}, D_{10}, C_u, C_c	all
Water content	ASTM D2216	w	all
Index test	ASTM D4318	PL, LL, PI	all
One dimensional consolidation	ASTM D2435	C_c, OCR	all
Resonant column test	ASTM 4015	G_{max}, G_d	D04, D10, D20, D30 S04, S10, S20, S30

Note: D_{60}, D_{50}, D_{30}, D_{10} mean: the diameter of the soil particles for which 60% , 50%, 30%, 10% of the particles are finer; C_u: uniformity coefficient; C_c: coefficient of curvature; PL means: plastic limit; LL: liquid limit; PI: plastic index; C_c : compression index, $=\frac{D_{60}}{D_{10}}$; OCR: overconsolidation ratio, $=\frac{(D_{30})^2}{D_{10}D_{60}}$; G_{max} : the maximum dynamic shear modulus; G_d: dynamic shear modulus.

Preprints (www.preprints.org) | NOT PEER-REVIEWED | Posted: 7 September 2023 doi:10.20944/preprints202309.0502.v1

3. Results and discussion

3.1. Physical property characterization

The test results provided a specific gravity (Gs) of 2.71 for the undisturbed loess and a Gs value of 2.72 for the landslide deposit. As depicted in Figure 4, both the undisturbed loess and the deposit exhibit a gradual increase in γ and $\gamma_d$with depth. However, at the same depth, the deposit's γ and γ_d surpass those of the undisturbed loess.

Analyzing the moisture content-depth curve, the undisturbed loess maintains a relatively stable and low moisture content at depths shallower than 10 meters. Between 10 and 20 meters, it experiences a gradual rise in moisture content, followed by a rapid surge in moisture below 20 meters. The saturation level reaches approximately 80% at a depth of 30 meters. In contrast, the deposit at the same depth showcases higher saturation than the undisturbed loess, with its moisture content uniformly increasing as depth grows. At 30 meters deep, the saturation level approaches 90%.

The alterations in the physical properties of these two materials stems from notable changes in their porosity. The undisturbed loess, known for being a wind-blown soil with large pores, loose structure, and weak cohesion, exhibits a surface porosity ratio of 1.3. With greater depth, this ratio decreases, reaching 0.86 at 30 m deep, while still maintaining its character as a porous and loosely packed soil. Conversely, at the same depth, the deposit's porosity ratio is significantly lower than that of the undisturbed loess. It reaches a maximum of 0.89 at the surface and declines with depth, reaching only 0.58 at a depth of 30 m.

This suggests that the loose and porous structure of the undisturbed loess becomes disrupted after undergoing the seismic landslide process. After deposition, the landslide deposit experiences reduced porosity, a compacted structure, increased density, and dry density.

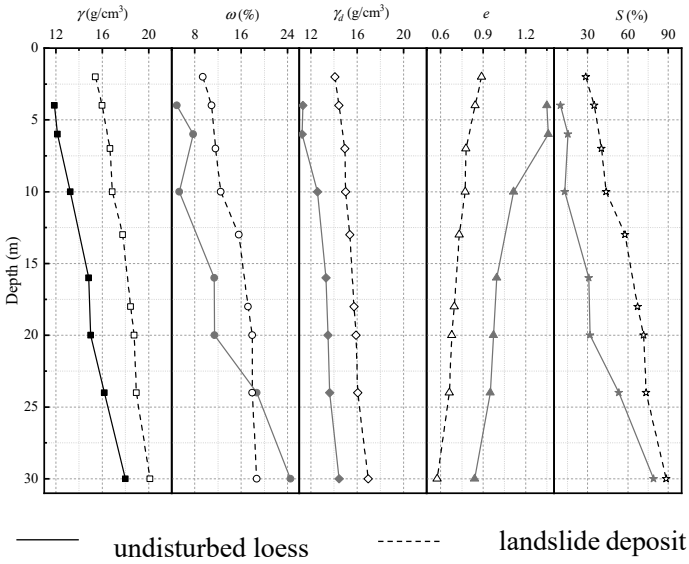

Figure 4. Density, water content, dry density, initial void ratio and saturation degree of undisturbed loess and landslide deposit at different depths.

The grain size distribution was presented in Figure 5. The results showed that the samples of undisturbed loess in slope contain 8.1%~14.8% of clay （<0.002mm）, 80.0%~84.2% of silt (0.002-0.075mm), and 3.8%~7.7% of sand (0.075-0.25mm). At a depth of 30 meters, the soil sample exhibits the highest concentration of sand and the lowest concentration of clay. The samples of deposits contain 12.3%~17.3% of clay（<0.002mm）, 77.1%~84.5% of silt (0.002-0.075mm), and 1.6%~6.3% of sand (0.075-0.25mm). Compared to the undisturbed loess, the landslide deposits exhibit an increase in the clay particle content and a decrease in the sand particle content.

Preprints (www.preprints.org) | NOT PEER-REVIEWED | Posted: 7 September 2023 doi:10.20944/preprints202309.0502.v1

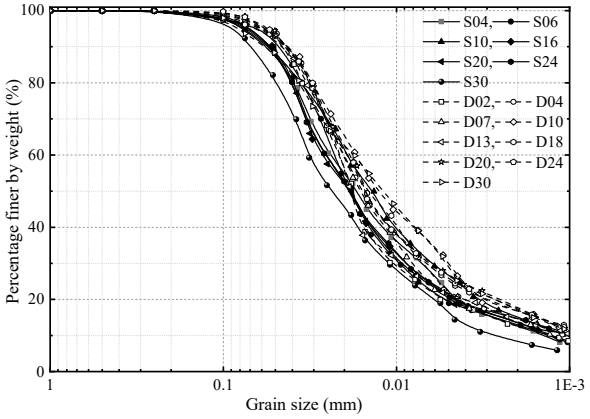

Figure 5. Grain size distribution curve of undisturbed loess and landslide deposit in different depths.

The particle size distributions of the two sample types, undisturbed loess and landslide deposits, were subjected to statistical analysis by measuring their *D60*, *D50*, *D30*, and *D10* values at different depths. The results depicted in Figure 6 indicate that, for the undisturbed loess, the *D60* values display a fluctuating pattern with depth, ranging between 19.5μm and 33.2μm. The *D50*, *D30*, and *D10* values exhibit relatively minor variations with depth, except for a more significant shift at a depth of 30m.

In contrast, the landslide deposits exhibit consistent *D60*, *D50*, *D30*, and *D10* values at various depths. When compared to the undisturbed loess, the landslide deposits display relatively uniform *D60*, *D50*, *D30*, and *D10* values above a depth of 15m. However, beyond the 15m mark, the *D60*, *D50*, *D30*, and *D10* values of the landslide deposits decrease, with the reductions being particularly pronounced for *D60*, *D50*, and *D30*.

Simultaneously, both the undisturbed loess and the landslide deposits have relatively high uniformity coefficients (C_u>4), and their coefficients of curvature (C_c>1) are also large. This indicates a wider distribution of particle sizes, implying a well-graded nature. In such cases, the soil particles exhibit significant variations in size, encompassing both larger and smaller particles.

Preprints (www.preprints.org) | NOT PEER-REVIEWED | Posted: 7 September 2023 doi:10.20944/preprints202309.0502.v1

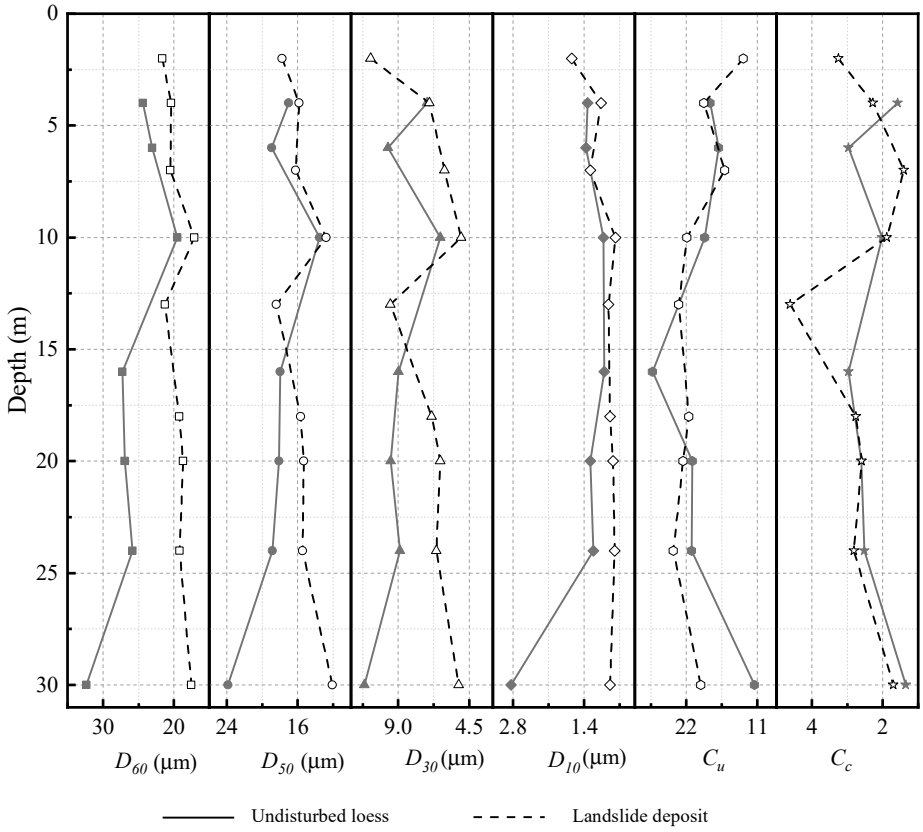

Figure 6. The different diameter of undisturbed loess and landslide deposit in different depths.

In Table 2, the average *D60*, *D50*, *D30*, and *D10* values of the landslide deposits are smaller than those of the undisturbed loess by 6.1μm, 1.3μm, 1.8μm, and 0.4μm, respectively. After experiencing seismic sliding, the larger particles in the soil have reduced. The coefficient of variation indicates that the particle size differences at various depths of the landslide deposits are minimal, suggesting that the particles have become more uniform across different depths due to the soil sliding process.

Table 2. Mean value and coefficient of variation of grain size distribution of undisturbed loess and landslide deposit.

		D_{60} (μm)	D_{50}(μm)	D_{30}(μm)	D_{10}(μm)	C_u	C_c
Samples in Slope	Mean value	25.6	18.3	8.8	1.4	19.3242	2.2822
	Coefficient of variation	0.1549	0.1680	0.1821	0.4366	0.2490	0.2833
Samples in deposit	Mean value	19.5	15.5	7.0	1.0	20.1573	2.5852
	Coefficient of variation	0.0811	0.1309	0.2721	0.2729	0.1766	0.3723

Soils with a higher proportion of smaller particles typically exhibit higher liquid limits. As shown in Figure 7, according to Gibbs' classification method based on liquid limit and plasticity index, both the undisturbed loess and landslide deposit fall between the A-line and U-line. The undisturbed loess has a lower liquid limit, closer to silty loess, while the landslide deposit has a higher liquid limit, closer to clayey loess. The liquid limit test results are consistent with the particle analysis results.

Preprints (www.preprints.org) | NOT PEER-REVIEWED | Posted: 7 September 2023 doi:10.20944/preprints202309.0502.v1

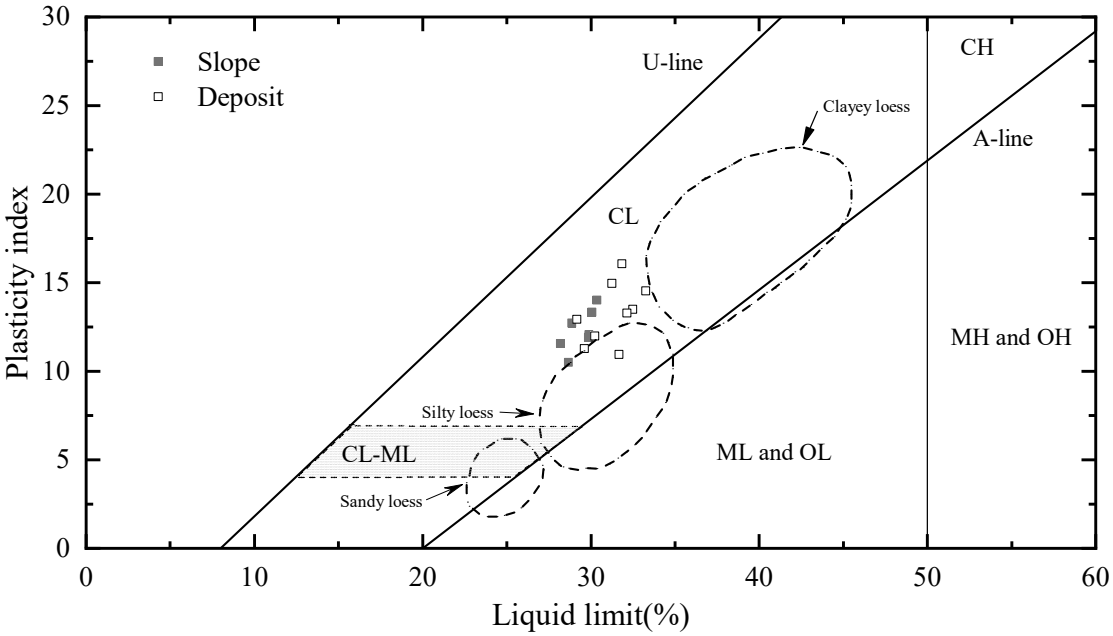

Figure 7. Trends of plasticity characteristics of undisturbed loess and landslide deposit.

Based on the variations in pore structure and particle size of the undisturbed loess and landslide deposits, it can be inferred that during the occurrence and movement of a landslide, the loose and porous structure of the undisturbed loess undergoes fragmentation. Larger soil particles experience compression, friction, fragmentation, and abrasion during their movement, resulting in the formation of smaller particles. Additionally, as the landslide progresses, continuous collisions among larger particles cause them to move downward, leading to further fragmentation and abrasion. Simultaneously, smaller particles are more easily transported by the surrounding soil and water flow, tending to settle in the lower sections of the landslide deposit. Consequently, the lower parts of the landslide deposit might contain a higher proportion of smaller particles. This phenomenon can be attributed to the combined effects of the fragmentation and abrasion of larger particles during their movement and the selective transportation and deposition of particles of different sizes during the landslide process.

3.2. Consolidation characterization

The intact loess is a type of soil with strong structural strength and low initial density, and its mechanical properties are closely related to its structural characteristics. Its compression and plasticity characteristics also differ from other types of soils. The present study investigated the undisturbed loess and landslide deposit soil using standard consolidation test. The soil samples were subjected to consolidation at different pressure levels (12.5, 25, 50, 100, 200, 300, 400, 600, 800 kPa), and the rebound ratio of each level was recorded after 24 hours of unloading. The void ratio of the samples after consolidation is e_i,

$$e_i = e_0 - \frac{1+e_0}{h_0}\Delta h_i \quad (1)$$

In the equation, e_0 represents the initial void ratio, h_0 represents the initial height of the soil sample, and Δh_i represents the deformation of the sample after achieving consolidation stability under a certain level of pressure.

The experimental data were processed using the da & de's [30] program and the Casagrande's [31] method was used to plot the compression curve, from which the compression index, pre-consolidation pressure (P_c), and over-consolidation ratio (OCR) were determined.

 doi:10.20944/preprints202309.0502.v1

$$OCR = \frac{p_c}{p_0} \quad (2)$$

p_c is the maximum vertical effective stress that a soil was subjected to in the past, p_0 is existing vertical effective stress.

The undisturbed loess has a strong structural behavior at low water content, which is manifested as a state of over-consolidation, i.e. *OCR* is much greater than 1. As the water content of the soil sample increases, the structural behavior of the loess gradually weakens, and *OCR* tends to approach 1, which is manifested as normal consolidation [32]. As shown in Figure 8, the initial pre-consolidation pressure of the undisturbed loess is notably higher than the vertical stress at depths exceeding 5 meters. With increasing depth and moisture content, the pre-consolidation pressure and vertical stress gradually converge. This trend aligns with the typical understanding of the dynamic consolidation pressure in loess. The compression index ranges from 0.13 to 0.33, indicating a soil of moderate compressibility.

The upper layer (above 5 meters) of the landslide deposit still maintains a pronounced structural behavior, whereas the vertical stress of soil samples at depths of 10 meters and below progressively surpasses the pre-consolidation pressure. Consequently, the consolidation state shifts from over-consolidation at the surface to normal consolidation and eventually to under-consolidation. The compression coefficient of soil samples at shallow depths ranges from 0.17 to 0.22, indicating moderate compressibility characteristics. Meanwhile, the compression coefficient of soil samples at greater depths varies from 0.08 to 0.1, signifying low compressibility characteristics.

The intact loess experiences a significant alteration in its compression properties as its structure gets disrupted during the sliding process and undergoes consolidation after deposition. The upper layer of the intact loess demonstrates characteristics of over-consolidated, under-compacted soil behavior at low water content, while the deeper layer shows characteristics of normally consolidated, under-compacted soil behavior at higher water content. The upper part of the landslide deposit exhibits over-consolidated, low-compression characteristics, whereas the lower part shows characteristics of under-consolidation with low compression. This phenomenon can be attributed to the greater compression and shear experienced by the deep-seated slide mass during movement, leading to more severe soil disruption, destruction of loess structure, reduced porosity, and tighter particle arrangement. Furthermore, the landslide deposit has undergone nearly a century of substantial re-consolidation, but its deep layers still exhibit under-consolidated features. Thus, for engineering construction on such deposits, attention should be paid to the compression characteristics of the deep soil layers.

Preprints (www.preprints.org) | NOT PEER-REVIEWED | Posted: 7 September 2023 doi:10.20944/preprints202309.0502.v1

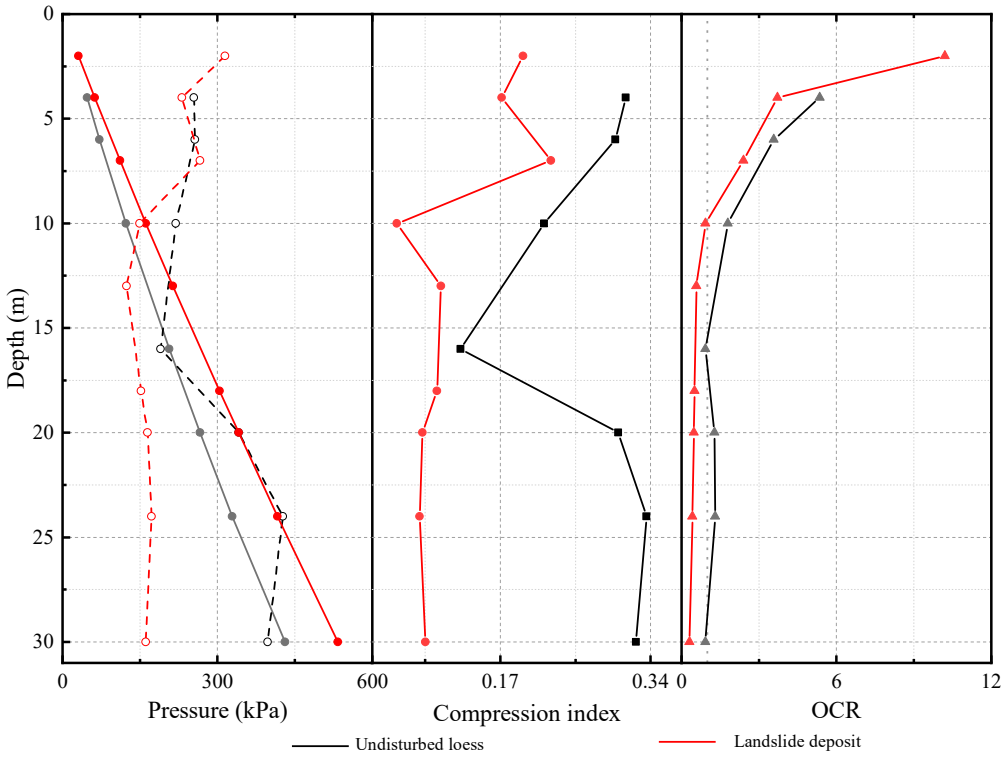

Figure 8. The compression index and OCR of undisturbed loess and landslide deposit in different depths.

3.3. Dynamic Shear Modulus Characteristics

Loess has long been a focus of researchers due to its strong sensitivity to water and vulnerability to earthquakes, particularly in terms of its dynamic properties, such as the dynamic shear modulus. However, little research has been done on whether the dynamic properties of the deposited soil mass change significantly after experiencing a landslide.

We normalized the results using G/G_{max}-γ, and the experimental and fitting results are shown in the Figure 9 , soil samples of *D04*, *D10*, *D20*, *D30* and *S04*, *S10*, *S20*, *S30* were subjected to resonant column tests with varying confining pressures of 50, 100, 200, and 300 kPa. T The trends in the changes of loess and landslide deposits under different consolidation pressures were similar, with the attenuation rate slowing down as the confining pressure increased. The attenuation of intact loess was slower than that of landslide deposits at the same burial depth. The G/G_{max}-γ of intact loess had a larger variation range than that of landslide deposits under different confining pressures, indicating the pressure sensitivity of intact loess, especially at depths of 4m and 20m. At a depth of 30m, the curves for both the undisturbed loess and the landslide deposit are relatively similar.

The test results were processed using Hardin's model [33,34] to obtain the maximum dynamic shear modulus (G_{max}) of the soil samples. As shown in the Figure 10(a), both the undisturbed loess and the landslide deposit exhibit an increase in their dynamic shear modulus (G_{max}) with rising confining pressures. Nevertheless, across various depths, the G_{max} of the intact loess and the landslide deposit doesn't exhibit significant differences in most cases. There is an exception in the S10 depth group, where the G_{max} is notably higher than the other depth groups. Within soil samples taken from different depths of both loess and landslide deposits, the rate of change in dynamic shear modulus with increasing confining pressure varies. Notably, for the intact loess with pronounced structural characteristics, the rate of change is slower in the upper layers compared to deeper layers when subjected to increasing confining pressures.

Furthermore, the G_{max} acquired through the shear wave velocity method surpasses values obtained from conventional laboratory tests. This suggests that the shear wave velocity method is

Preprints (www.preprints.org) | NOT PEER-REVIEWED | Posted: 7 September 2023 doi:10.20944/preprints202309.0502.v1

more sensitive and capable of providing a more accurate measurement of the maximum dynamic shear modulus of soil.

The moisture content is one of the key control factors for the maximum dynamic shear modulus of loess. Song's [35] experimental results showed that the maximum dynamic shear modulus of loess increased in three stages as the moisture content increased. When the moisture content of the loess is below its plastic limit, the dynamic shear modulus (G_{max}) decreases with increasing moisture content. When the moisture content of the loess approaches its plastic limit, G_{max} undergoes a sharp decrease, reaching its maximum attenuation rate. As the moisture content of the loess further increases and exceeds its plastic limit, the attenuation trend of G_{max} slows down and gradually stabilizes, even approaching saturation. Under low confining pressures, the initial dynamic shear modulus G_{max} of the intact loess exhibits relatively weak sensitivity to water content, but as the confining pressure increases, the water sensitivity of the loess becomes more pronounced.

In this study, as shown in the Figure 10(b), when the moisture content of the intact loess is below its plastic limit, G_{max} initially increases and then rapidly decreases as the moisture content increases. With further increases in moisture content, the rate of G_{max} attenuation slows down, and G_{max} gradually stabilizes as it approaches saturation. This trend remains consistent under different confining pressures. However, the landslide deposit is less sensitive to changes in moisture content, and the attenuation trend of G_{max} is relatively gradual. Regardless of the confining pressure, the G_{max} of the landslide deposit is greater than that of the intact loess at the same moisture content. The results indicate that the sensitivity of the landslide deposit to moisture content is weaker compared to intact loess. This difference in sensitivity could be attributed to variations in material composition, particle arrangement, and structural characteristics of the deposit.

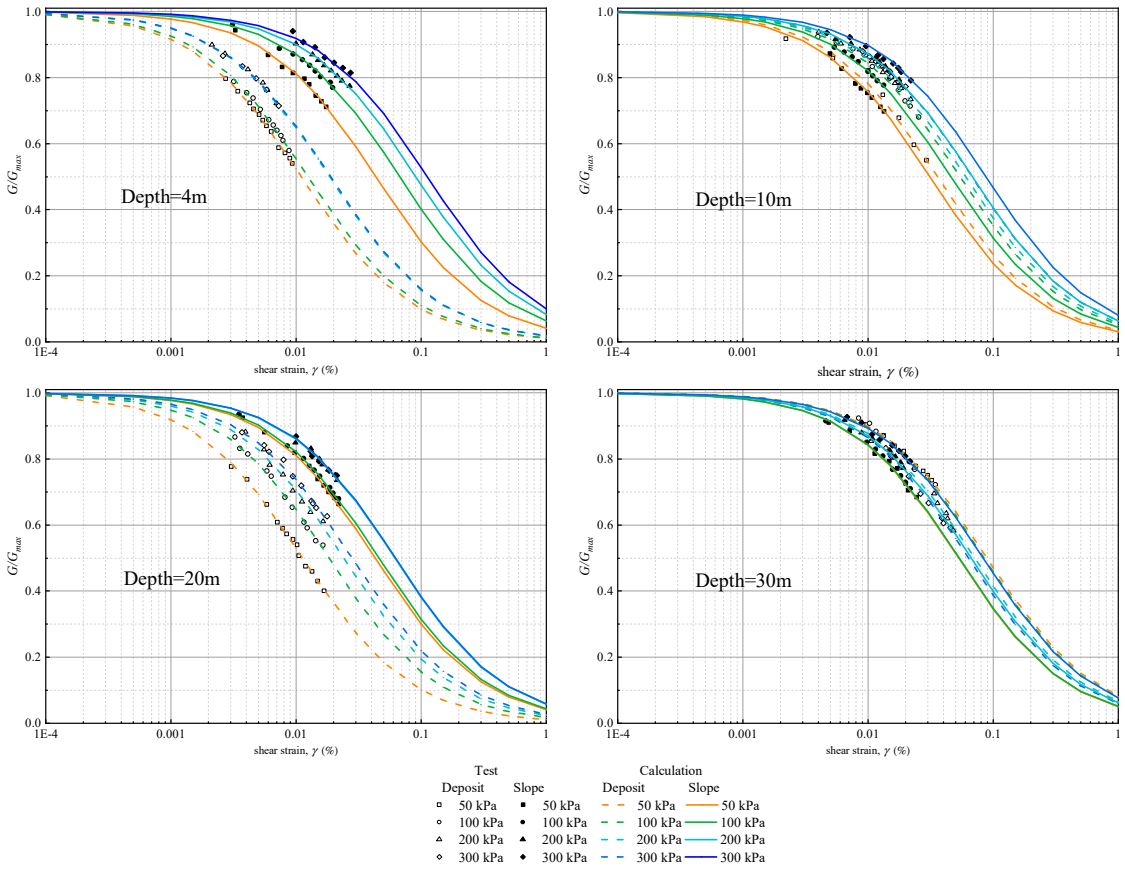

Figure 9. Dynamic shear modulus ratio and dynamic shear strain curve of undisturbed loess and landslide deposit in different depths.

Preprints (www.preprints.org) | NOT PEER-REVIEWED | Posted: 7 September 2023 doi:10.20944/preprints202309.0502.v1

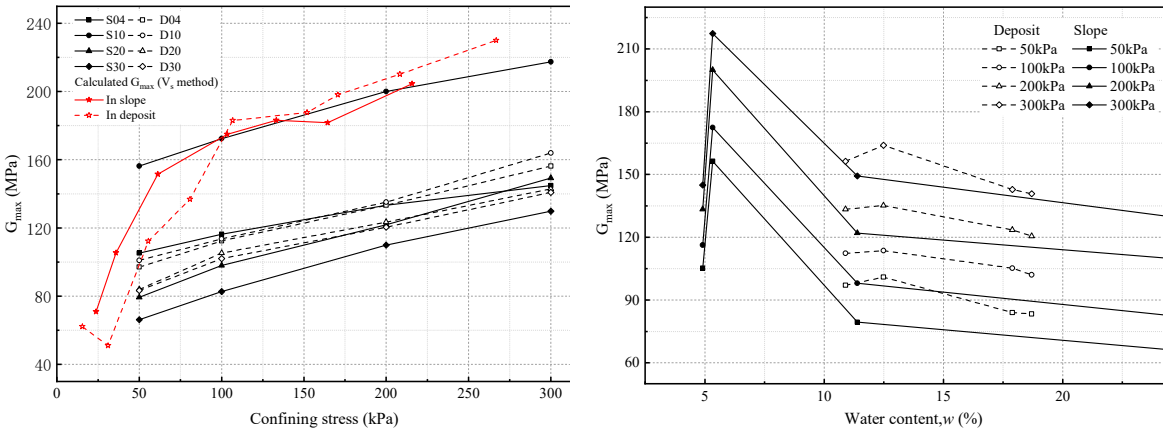

(a) (b)

Figure 10. (a) mean effective confining pressure with the maximum dynamic shear modulus (Gmax) of undisturbed loess and landslide deposit (b) water content w (%) with the maximum dynamic shear modulus (Gmax) of undisturbed loess and landslide deposit.

The Gmax of soil is a crucial parameter for assessing the deformation and failure characteristics of soil under dynamic loading. It holds significant importance in various fields including engineering design, seismic disaster prediction, underground structure design, and foundation engineering. It is closely related to factors such as soil porosity, confining pressure, and the OCR. A Power empirical equation were developed by Hardin and Black [36] and Hardin [37], which considers the influence of pressure, void ratio and over-consolidation ratio on Gmax:

$$G_{max} = 625 \frac{A*OCR^k}{0.3+0.7e^2} P_a \left(\frac{\sigma_c'}{P_a}\right)^m \quad (3)$$

where σ_c' is effective mean normal stress (kPa), P_a is atmospheric pressure(kPa), k is the function of the plasticity index I_p, When I_p=0, 20, 40, 60, 80 and ≥100, k= 0.0, 0.18, 0.31, 0.41, 0.48 and 0.5. Considering the fact that the over-consolidation characteristics of the undisturbed loess are irrelevant to the stress history, and no additional OCR issue is required, therefore, the OCR values of the undisturbed loess are all 1. In addition, the soil at 4m of landslide deposit also exhibits the over-consolidation characteristics which are still related to its structural properties, and thus the OCR value is also 1.

The fitting results for the undisturbed loess and landslide deposit are obtained, as shown in Table 3. The differences in A and m values of undisturbed loess with depth reflect the longitudinal variability of soil properties. The A and m values of the landslide deposit exhibit relatively uniform changes, continuously increasing with depth and water content. In comparison to undisturbed loess, the A and m values of the landslide deposit have undergone significant variations longitudinally, characterized by a noticeable increase in A value. Notably, the m value is smaller than that of shallow-depth, low-water content undisturbed loess and larger than that of deep-depth, high-water content undisturbed loess.

Table 3. Fitting parameters of Hardin and Black equation for undisturbed loess and landslide deposit.

Sample	*Water content (%)*	*OCR*	*k*	*A*	*m*	*Correlation coefficient R^2*
S04	4.91	5.36		1322	0.1820	0.994
S10	5.33	1.79		2869	0.1895	0.993
S20	11.39	1.28		2002	0.3563	0.987
S30	24.5	0.92		2008	0.3875	0.998
D04	10.9	3.71		2802	0.2685	0.987

D10	12.49	0.92	0.12	3224	0.2773	0.954
D20	17.89	0.48	0.13	3570	0.2873	0.993
D30	18.7	0.30	0.12	4263	0.2882	0.992

The correlation coefficient of the fitting results indicates that the predicted parameters are reasonable, and these parameters can provide references for the maximum dynamic shear modulus of soils at different depths in this region.

4. Conclusions

A series of tests were conducted to reveal the differences in particle size distribution, liquid limit, consolidation characteristics, and maximum dynamic shear modulus between undisturbed loess and landslide deposits. The following conclusions can be summarized:

1. The process of landslide has disrupted the original structure of the loess, leading to a reduction in its porosity and a densification of the soil. This change in structural characteristics results in significant differences in physical properties between landslide deposits and undisturbed loess. This process also causes abrasion and sieving of loess particles, leading to the transformation of larger particles into smaller ones and forming a more uniform particle size distribution. Within the landslide deposits, the movement and segregation of particles lead to variations in particle size distribution in different parts.

2. The disruption of structure and changes in particle size significantly affect the consolidation characteristics of landslide deposits, leading to a substantial reduction in their compression coefficient. The study also found that despite experiencing nearly a hundred years of consolidation, the soil in the middle and lower parts of the landslide deposits still exhibits under-consolidated behavior.

3. Although the differences in maximum dynamic shear modulus between different depths of undisturbed loess and landslide deposits are relatively small, due to variations in porosity, consolidation characteristics, etc., their dynamic shear modulus decay rates are faster than that of the undisturbed loess. This emphasizes the need to consider the differences in their physical properties when assessing the deformation and failure characteristics of these two types of soil under dynamic loading. Furthermore, fitting parameters (A and m values) were derived from experimental results to predict the maximum dynamic shear modulus of both loess and landslide deposits in the region.

Data availability: All data, models, or codes that support the findings of this study are available from the corresponding author upon reasonable request.

Acknowledgments: This work is financially supported by the National Natural Science Foundation of China (No. U1939209), Scientific Research Fund of Institute of Engineering Mechanics, China Earthquake Administration (Grant NO.2020EEEVL0201).

Declarations: The authors declare no competing interests.

References

1. Xianmo, Z., Yushan, L., Xianglin, P., & Shuguang, Z. Soils of the loess region in China. Geoderma **1983**, 29(3), 237-255.
2. Lanmin, Wang, Xiaowu, Pu, Jinchang, Chen. Distribution Characteristics and Disaster Risk of Earthquake Induced Landslides in the Loess Plateau. City and disaster reduction **2019**, 126(03):33-40.
3. Xu, Y., Allen, M. B., Zhang, W., Li, W., & He, H. Landslide characteristics in the Loess Plateau, northern China. Geomorphology **2020**, 359, 107150.
4. Close, U., McCormick, E. Where the mountains walked. National Geographic Magazine 1922. 41, 445–464.
5. Xu, Y., Liu-Zeng, J., Allen, M. B., Zhang, W., & Du, P. Landslides of the 1920 Haiyuan earthquake, northern China. Landslides **2021**, 18, 935-953.
6. Zhuang, J., Peng, J., Xu, C., Li, Z., Densmore, A., Milledge, D., Iqbal, J., Cui, Y.. Distribution and characteristics of loess landslides triggered by the 1920 Haiyuan Earthquake, Northwest of China. Geomorphology 2018, 314, 1–12.

7. Lanzhou Institute of Seismology, SSB, Seismic Crew of Ningxia Hui Autonomous Region. AD 1920 Haiyuan great earthquake. Seismological Press, Beijing, China, 1980.
8. Zhang, Z., & Wang, L. Geological disasters in loess areas during the 1920 Haiyuan Earthquake, China. GeoJournal **1995**, 36, 269-274.
9. Chang, C., Bo, J., Qi, W., Qiao, F., & Peng, D. Distribution of large-and medium-scale loess landslides induced by the Haiyuan Earthquake in 1920 based on field investigation and interpretation of satellite images. Open Geosciences **2022**, 14(1), 995-1019.
10. Puri, V. K. Liquefaction behavior and dynamic properties of loessial (silty) soils. University of Missouri-Rolla,1984.
11. Ishihara, K., Okusa, S., Oyagi, N., & Ischuk, A. Liquefaction induced flow slide in the collapsible loess deposit in Soviet Tajik. Soils and foundations **1990**, 30(4), 73-89.
12. He Guang, Zhu Hongbo. Study on loess seismic settlement. Journal of Geotechnical Engineering **1990**, (06), 99-103.
13. Wang, J., Gu, T., Zhang, M., Xu, Y., & Kong, J. Experimental study of loess disintegration characteristics. Earth Surface Processes and Landforms **2019**, 44(6), 1317-1329.
14. Varnes, D. J. Slope movement types and processes. Special report, 176, 11-33, 1978.
15. Wang Jiading, Zhang Zhuoyuan. Mechanism study of earthquake-induced high-speed loess landslides. Journal of Geotechnical Engineering **1999**, (06): 670-674.
16. Zhang, Z., & Duan, R. Discussion on seismic subsidence of loess sites in the northwest of China during earthquakes. In Proceedings of the International Symposium on Engineering Geology 1986, Problems of Seismic Areas (Vol. 2, pp. 65-76).
17. Seed, H. B., & Martin, G. R. The seismic coefficient in earth dam design. Journal of the Soil Mechanics and Foundations Division **1966**, 92(3), 25-58.
18. ZHANG, D., TAKEUCHI, A., & SASSA, K. The Motion Characteristics of Loess Landslides Induced by the Haiyuan Earthquake in the Ningxua Province, China. Landslides **1995**, 32(1), 12-17_1.
19. Zhang, D., & Wang, G. Study of the 1920 Haiyuan earthquake-induced landslides in loess (China). Engineering Geology **2007**, 94(1-2), 76-88.
20. Wang, G., Zhang, D., Furuya, G., & Yang, J. Pore-pressure generation and fluidization in a loess landslide triggered by the 1920 Haiyuan earthquake, China: a case study. Engineering Geology **2014**, 174, 36-45.
21. Wang L. Loess Dynamics. Seismological Press, Beijing, China, 2003
22. Carey J M, McSaveney M J, Petley D N. Dynamic liquefaction of shear zones in intact loess during simulated earthquake loading[J]. Landslides **2017**, 14(3): 789-804.
23. Pei, X., Zhang, X., Guo, B., Wang, G., & Zhang, F. Experimental case study of seismically induced loess liquefaction and landslide. Engineering Geology **2017**, 223, 23-30.
24. Shanmugam, G., & Wang, Y. The landslide problem. Journal of Palaeogeography **2015**, 4(2), 109-166.
25. Cheng, C. H., Hsiao, S. C., Huang, Y. S., Hung, C. Y., Pai, C. W., Chen, C. P., & Menyailo, O. V. Landslide-induced changes of soil physicochemical properties in Xitou, Central Taiwan. Geoderma **2016**, 265, 187-195.
26. Zhang, L. M., Xu, Y., Huang, R. Q., & Chang, D. S. Particle flow and segregation in a giant landslide event triggered by the 2008 Wenchuan earthquake, Sichuan, China. Natural Hazards and Earth System Sciences **2011**, 11(4), 1153-1162.
27. Getahun, E., Qi, S. W., Guo, S. F., Zou, Y., & Liang, N. Characteristics of grain size distribution and the shear strength analysis of Chenjiaba long runout coseismic landslide. Journal of Mountain Science **2019**, 16(9), 2110-2125.
28. Li, Y., & Mo, P. A unified landslide classification system for loess slopes: A critical review. Geomorphology **2019**, 340, 67-83.
29. Huang, X., Cai, X., Bo, J. Experimental study of the influence of gradation on the dynamic properties of centerline tailings sand. Soil Dynamics and Earthquake Engineering **2021**, 151, 106993.
30. da Silva, A. R., & de Lima, R. P. Soil physics: an R package to determine soil preconsolidation pressure. Computers & geosciences **2015**, 84, 54-60.
31. Casagrande, A. Research on the Atterberg limits of soils, Public Roads **1932**, Vol. 13, No. 8, pp. 121–136.
32. Wang Q, Kong Y, Zhang X. Mechanical Effect of Pre-consolidation Pressure of Structural Behavior Soil[J]. Journal of Southwest Jiaotong University **2016**, (05), 987-994.
33. Hardin, B. O., & Drnevich, V. P. Shear modulus and damping in soils: design equations and curves. Journal of the Soil mechanics and Foundations Division **1972**, 98(7), 667-692.
34. Darendeli, M. B. Development of a new family of normalized modulus reduction and material damping curves. The university of Texas at Austin, 2001.
35. Song, B., Tsinaris, A., Anastasiadis, A., Pitilakis, K., & Chen, W. Small-strain stiffness and damping of Lanzhou loess. Soil Dynamics and Earthquake Engineering **2017**, 95, 96-105.
36. Hardin, B. O., & Black, W. L. Vibration modulus of normally consolidated clay. Journal of the Soil Mechanics and Foundations Division **1968**, 94(2), 353-369.

37. Hardin, B. O. The nature of stress-strain behavior for soils. In From Volume I of Earthquake Engineering and Soil Dynamics--Proceedings of the ASCE Geotechnical Engineering Division Specialty Conference, June 19-21, 1978, Pasadena, California. Sponsored by Geotechnical Engineering Division of ASCE in cooperation with: (No. Proceeding).